Naval Research Laboratory

Washington, DC 20375-5320

NRL/MR/6790--93-7320

(2)

Optically Guided Laser Wakefield Acceleration

ERIC ESAREY
PHILLIP SPRANGLE
JONATHAN KRALL
ANTONIO TING
GLENN JOYCE

Beam Physics Branch
Plasma Physics Division

April 19, 1993

REPORT DOCUMENTATION PAGE

Form Approved
OMB No. 0704-0188

1. AGENCY USE ONLY *(Leave Blank)*	2. REPORT DATE	3. REPORT TYPE AND DATES COVERED
	April 19, 1993	Interim

4. TITLE AND SUBTITLE

Optically Guided Laser Wakefield Acceleration

5. FUNDING NUMBERS

67-0899-03
DOE CONTRACT #
DOE-AI05-83ER40117

6. AUTHOR(S)

Eric Esarey, Phillip Sprangle, Jonathan Krall, Antonio Ting, and Glenn Joyce

7. PERFORMING ORGANIZATION NAME(S) AND ADDRESS(ES)

Naval Research Laboratory
Washington, DC 20375-5320

8. PERFORMING ORGANIZATION REPORT NUMBER

NRL/MR/6790--93-7320

9. SPONSORING/MONITORING AGENCY NAME(S) AND ADDRESS(ES)

Department of Energy, Washington, DC 20545
ONR, Arlington, VA 22217

10. SPONSORING/MONITORING AGENCY REPORT NUMBER

11. SUPPLEMENTARY NOTES

12a. DISTRIBUTION/AVAILABILITY STATEMENT

Approved for public release; distribution unlimited.

12b. DISTRIBUTION CODE

13. ABSTRACT ***(Maximum 200 words)***

The laser wakefiled acceleration concept is studied using a general axisymmetric formulation based on relativistic fluid equations. This formalism is valid for arbitrary laser intensities and allows the laser-plasma interaction to be simulated over long propagation distances (many Rayleigh lengths). Several methods for optically guiding the laser pulse are examined, including relativistic guiding, performed plasma density channels and tailored pulse profiles. Self-modulation of the laser, which occurs when the pulse length is long compared to the plasma wavelength and the power exceeds the critical power, is also examined. Simulations of three possible laser wakefield accelerator (LWFA) configurations are performed and discussed: (i) a channel-guided LWFA, (ii) a tailored-pulse LWFA, and (iii) a self-modulated LWFA.

14. SUBJECT TERMS

Laser-plasma
Electron accelerator
Wakefields

15. NUMBER OF PAGES

27

16. PRICE CODE

17. SECURITY CLASSIFICATION OF REPORT	18. SECURITY CLASSIFICATION OF THIS PAGE	19. SECURITY CLASSIFICATION OF ABSTRACT	20. LIMITATION OF ABSTRACT
UNCLASSIFIED	UNCLASSIFIED	UNCLASSIFIED	UL

NSN 7540-01-280-5500

Standard Form 298 (Rev. 2-89)
Prescribed by ANSI Std 239-18
298-102

CONTENTS

OPTICALLY GUIDED LASER WAKEFIELD ACCELERATION

I. INTRODUCTION

The possibility of utilizing the fields of an intense laser beam to accelerate particles to high energies has attracted a great deal of interest [1]. The study of laser driven accelerators is motivated by the ultrahigh fields associated with high intensity laser pulses. The peak amplitude of the transverse electric field of the laser pulse is given by

$$E_L[\mathrm{TV/m}] = 2.7 \times 10^{-9} I^{1/2}[\mathrm{W/cm^2}] = 3.2 a_0/\lambda[\mu\mathrm{m}], \tag{1}$$

where I is the laser intensity, λ is the laser wavelength, a_0 is the laser strength parameter, and linear polarization has been assumed. The laser strength parameter is related to the power, P, of a linearly polarized laser pulse by $P[\mathrm{GW}] = 21.5(a_0 r_0/\lambda)^2$, where r_0 is the minimum spot size of the Gaussian radial profile. Physically, a_0 is the normalized transverse quiver momentum of the electrons in the laser field, $a_0 = p_\perp/m_e c = \gamma v_\perp/c$, where γ is the relativistic factor and $v_\perp$ is the transverse electron velocity. Recent developments in compact laser systems [2,3] have resulted in laser pulses with ultrahigh powers, $P \gtrsim 10$ TW, ultrahigh intensities, $I \gtrsim 10^{18}$ W/cm^2, moderate pulse energies, $W \gtrsim 1$ J, and ultrashort pulse durations, $\tau_L \lesssim 1$ ps. For a laser wavelength of $\lambda = 1$ μm, $I \simeq 10^{18}$ W/cm^2 implies $a_0 \simeq 1$ and, hence, highly relativistic electron motion. The transverse electric field associated with this intensity is $E_L \simeq 3$ TV/m. Various laser acceleration concepts involve transforming a small fraction of the ultrahigh transverse laser field into an axial electric field which can be used to accelerate electrons.

A laser driven accelerator that has a number of attractive features is the laser wakefield accelerator (LWFA) [4-11]. In the LWFA, a short ($\lesssim 1$ ps) intense ($a_0 \gtrsim 1$) laser pulse propagates through an underdense plasma, $\lambda^2/\lambda_p^2 \ll 1$, where $\lambda_p = 2\pi c/\omega_p$ is the plasma wavelength, $\omega_p = (4\pi e^2 n_0/m_e)^{1/2}$ is the plasma frequency, and n_0 is the ambient plasma density. The ponderomotive force associated with the laser pulse envelope, $F_p \sim \nabla E_L^2$, expels electrons from the region of the laser pulse. If the laser pulse is sufficiently intense, virtually all of the plasma electrons will be expelled. When the laser pulse length, $L = c\tau_L$ (defined as twice the full width at half maximum of the intensity), is approximately equal to the plasma wavelength, $L \simeq \lambda_p$, large amplitude plasma waves (wakefields) will be excited with phase velocities approximately equal [12] to the laser pulse group velocity.

Manuscript approved February 19, 1993.

The axial and transverse electric fields associated with the wakefield can accelerate and focus a trailing electron beam. The ratio of the accelerating field, E_z, to the laser field in the LWFA is given by [6,7]

$$E_z/E_L \simeq 1.2 \times 10^{-11} n_0^{1/2}[\mathrm{cm}^{-3}]\lambda[\mu\mathrm{m}]a_0(1+a_0^2/2)^{-1/2}, \qquad (2)$$

where linear polarization has been assumed. For $n_0 = 10^{18}$ cm^{-3}, $a_0 = 1$ and $\lambda = 1$ μm, the accelerating field is $E_z \simeq 30$ GV/m, which is $\simeq 1\%$ of the laser field. In the LWFA, the plasma serves a dual purpose, it acts as a medium which (i) transforms a fraction of the laser field into an accelerating field and (ii) modifies the refractive index to optically guide the laser pulse.

In the absence of optical guiding, the interaction distance will be limited by diffraction [5]. In vacuum, the laser spot size, r_L, evolves according to $r_L = r_0(1+z^2/Z_R^2)^{1/2}$, where z is the axial propagation distance, $z = 0$ is the focal point, and $Z_R = \pi r_0^2/\lambda$ is the Rayleigh length. Diffraction limits the interaction distance to $\simeq \pi Z_R$. The maximum energy gain of the electron beam in a single stage, assuming vacuum diffraction, is $\Delta W \simeq \pi Z_R E_z$ which, in the limit $a_0^2 \ll 1$, may be written as $\Delta W \simeq 580(\lambda/\lambda_p)P$, where ΔW is in MeV and P is in TW [7]. As an example, consider a $\tau_L = 200$ fs linearly polarized laser pulse with $P = 10$ TW, $\lambda = 1$ μm and $r_0 = 30$ μm ($a_0 = 0.72$). The requirement that $L \simeq \lambda_p$ implies a plasma density of $n_0 = 3 \times 10^{17}$ cm^{-3}. The wakefield amplitude is $E_z = 10$ GV/m and the interaction length is 0.9 cm. Hence, a properly phased tailing electron bunch could gain an energy of $\Delta W = 90$ MeV in a single stage without optical guiding.

The interaction length and consequently the electron energy gain, may be greatly increased by optically guiding the laser pulse in the plasma. Optical guiding in plasmas can be achieved by relativistic effects [5-11,13-16], preformed density channels [7-9,17] or tailored laser pulse profiles [8-10]. Numerical simulations of three LWFA configurations which utilize optical guiding will be presented: (i) a channel-guided LWFA [9], (ii) a tailored-pulse LWFA [10], and (iii) a self-modulated LWFA [11].

The remainder of this paper is organized as follows. In Section II, a nonlinear, relativistic fluid model is presented which describes the intense laser-plasma interaction. This model is valid for arbitrary laser intensities and is capable of simulating, in the ax-

isymmetric limit, laser pulse propagation over large distances (many Rayleigh lengths). Various optical guiding mechanisms are briefly described in Section III, including relativistic optical guiding, long pulse self–modulation, tailored pulse propagation, and preformed plasma density channels. In Section IV, numerical simulations of a channel–guided LWFA, a tailored–pulse LWFA, and a self–modulated LWFA are presented. A summary is given in Section V.

II. NONLINEAR FORMULATION

The large differences between the laser wavelength and other characteristic longitudinal lengths in the system, i.e., laser propagation distance, laser pulse length and plasma wavelength, make the direct numerical integration of the dynamical equations over extended distances impractical. In the following, a fully nonlinear, relativistic, two–dimensional axisymmetric laser–plasma propagation model is formulated and numerically evaluated for laser pulses of ultrahigh intensities and arbitrary polarizations [8-11]. The formulation has a number of unique features which allow numerical simulations to be carried out over extended laser propagation distances. The appropriate Maxwell–fluid equations are recast into a convenient form by (i) performing a change of variables to the "speed of light" coordinates, (ii) applying the quasi-static approximation (QSA) [6], (iii) expanding in two small parameters (which are independent of the laser intensity) and (iv) averaging over the fast spatial scale length, i.e., the laser wavelength.

The plasma is modelled using relativistic cold fluid equations. The fields associated with the intense laser–plasma interaction may be described by the normalized scalar and vector potentials, $\phi = e\Phi/m_e c^2$ and $\mathbf{a} = e\mathbf{A}/m_e c^2$, respectively. In the following, the Coulomb gauge is used, $\nabla \cdot \mathbf{a} = 0$, the ions are assumed stationary and thermal effects are neglected. It is convenient to introduce the normalized fluid momentum $\mathbf{u} = \gamma \mathbf{v}/c$ and the fluid quantity $\rho = n/(n_0\gamma)$, where $\mathbf{v}$ is the electron fluid velocity, $\gamma = (1+u^2)^{1/2}$ is the relativistic factor of the electron fluid, and n is the electron fluid density. In the fluid limit, the electron current is given by $\mathbf{J} = -en\mathbf{v}$ and the normalized wave equation is given by

$$\left(\nabla^2 - \frac{1}{c^2}\frac{\partial^2}{\partial t^2}\right)\mathbf{a} = k_p^2 \rho \mathbf{u} + \frac{1}{c}\frac{\partial}{\partial t}\nabla\phi, \tag{3}$$

where $k_p = \omega_p/c$. Poisson's equation is given by $\nabla^2\phi = k_p^2(\gamma\rho - \rho^{(0)})$, where $\rho^{(0)} = n^{(0)}/n_0$ and $n^{(0)}(r)$ is the initial plasma density profile (prior to the laser interaction) which can be a function of radial position. In the cold fluid limit, the electron response is determined by the the continuity equation, $\partial(\rho\gamma)/\partial t + c\nabla\cdot(\rho\mathbf{u}) = 0$, and the momentum equation, which can be written in the form

$$\frac{1}{c}\frac{\partial}{\partial t}(\delta\mathbf{u}) = \nabla(\phi - \gamma) + \frac{1}{\gamma}\mathbf{u}\times(\nabla\times\delta\mathbf{u}), \tag{4}$$

where $\delta\mathbf{u} = \mathbf{u} - \mathbf{a}$. Equation (4) also implies that the quantity $\mathbf{h} = \nabla\times\delta\mathbf{u}$ is zero provided it is initially zero [16]. Hence, the last term on the right side of Eq. (4) will be neglected.

The Maxwell–fluid equations can be simplified by the following. The full set of equations is recast into speed of light coordinates by introducing the independent variables $\zeta = z - ct$ and $\tau = t$. The QSA is then applied [6]. In the QSA, the electron transit time through the laser pulse ($\simeq \tau_L$) is assumed to be short compared to the laser pulse evolution time, which is determined by the pulse diffraction time, Z_R/c, or by the pulse dispersion time, ω/ω_p^2, where ω is the laser frequency. In the QSA, the electrons experience essentially static fields, allowing the $\partial/\partial\tau$ derivatives to be neglected in the fluid equations, but not in the wave equation. Within the QSA, the quantity $\gamma - u_z - \phi + a_z$ is an invariant which is set equal to unity, i.e., its value prior to the arrival of the laser pulse. Hence, $\gamma - u_z = 1 + \psi$, where $\psi = \phi - a_z$ is the wake potential. The resulting equations are expanded to first order in the parameters $\epsilon_1 = 1/kr_L \ll 1$ and $\epsilon_2 = k_p/k \ll 1$, where $k = 2\pi/\lambda$. All the fluid and field quantities are expanded in slow and fast terms, i.e., $Q = Q_s + Q_f$, where $|\partial Q_f/\partial\zeta| \sim |kQ_f|$ and $|\partial Q_s/\partial\zeta| \sim |k_pQ_s|$. Within this representation, the nonlinear fluid equations are averaged over the laser wavelength in the ζ,τ frame. The ζ–averaging allows for all the laser–plasma response quantities to be evaluated on the slow spatial scale, i.e., λ_p or L, permitting solutions over extended propagation distances.

The resulting equations describe the slowly varying components of the fluid and field quantities [8-11]:

$$\nabla_\perp^2\mathbf{a} = k_p^2\rho\mathbf{u} - \frac{\partial}{\partial\zeta}\nabla\phi, \tag{5a}$$

$$\left(\nabla_\perp^2 + \frac{\partial^2}{\partial\zeta^2}\right)\phi = k_p^2\left(\gamma\rho - \rho^{(0)}\right), \tag{5b}$$

$$\frac{\partial}{\partial \zeta}(\mathbf{u}-\mathbf{a}) = \nabla(\gamma-\phi), \tag{5c}$$

where the subscript s, denoting the slow component of the quantity, has been dropped. Equations (5a-c) represent, respectively, the slow components of the wave, Poisson's, and momentum equations. The slow component of the continuity equation follows from the divergence of Eq. (5a). The slow component of the relativistic factor is

$$\gamma = \frac{1+u_\perp^2+|\hat{a}_f|^2/2+(1+\psi)^2}{2(1+\psi)}. \tag{6}$$

In Eq. (6) and throughout the remainder of this paper, a linearly polarized laser pulse with amplitude $|\hat{a}_f|$ is assumed. The transverse component of the laser radiation field is $\mathbf{a}_f = \hat{\mathbf{a}}_f(r,\zeta,\tau)\exp(ik\zeta)/2+$ c.c., where $\hat{\mathbf{a}}_f$ is the complex, slowly varying amplitude, which satisfies the wave equation

$$\left[\nabla_\perp^2 + \frac{2}{c}\left(ik+\frac{\partial}{\partial\zeta}\right)\frac{\partial}{\partial\tau} - \frac{1}{c^2}\frac{\partial^2}{\partial\tau^2}\right]\hat{\mathbf{a}}_f \simeq k_p^2\rho\hat{\mathbf{a}}_f. \tag{7}$$

Typically, the last term on the left of Eq. (7) is small and can be neglected, as is done in the simulations discussed below. Within the QSA, the self-consistent, slowly varying equations in the ζ,τ variables, describing the laser-plasma interaction, to first order in ϵ_1 and ϵ_2, are given by Eqs. (5)-(7).

Equations (5a)-(5c) can be combined to yield a single equation for ψ in terms of $|\hat{a}_f|^2$ of the form $\partial^2\psi/\partial\zeta^2 = G(\psi,|\hat{a}_f|^2)$, where G is an involved function [8-11]. The equation for ψ is obtained by noting that $(1+\psi)\rho = \rho^{(0)} + k_p^{-2}\nabla_\perp^2\psi$ and $k_p^2\rho\mathbf{u}_\perp = \nabla_\perp\partial\psi/\partial\zeta$, assuming axisymmetry. Note also that the refractive index is solely a function of ψ through ρ, i.e., $\eta_R = 1 - k_p^2\rho/2k^2$. Equation (7) together with $\partial^2\psi/\partial\zeta^2 = G$ completely describe the 2D–axisymmetric, quasi–static laser–plasma interaction. In this axisymmetric model, the effects of various instabilities, such Raman sidescatter and stimulated backscatter, will be neglected [15,18,19]. The wake potential, ψ, is related to the axial electric field, E_z, of plasma response (wakefield) by $\hat{E}_z = -\partial\psi/\partial\zeta$, where $\hat{E}_z = eE_z/m_ec^2$. Furthermore, Eqs. (5)-(7), in the appropriate limits, reduce to models which have been previously studied. In the broad pulse limit, $\nabla_\perp \to 0$, Eqs. (5)-(7) reduce to a set of coupled equations describing the well–know one–dimension model [6,20]. In the limit $\partial/\partial\zeta \to 0$, Eqs. (5)-(7) reduce to a single equation describing the evolution of a long, axially uniform pulse [14].

III. OPTICAL GUIDING MECHANISMS

The optical guiding mechanisms discussed below are based on the principle of refractive guiding. Refractive guiding becomes possible when the radial profile of the index of refraction, $\eta_R(r)$, exhibits a maximum on axis, i.e., $\partial\eta_R/\partial r < 0$. The general expression for the index of refraction for a large amplitude electromagnetic wave in a plasma is given by $\eta_R \simeq 1 - \omega_p^2\rho(r)/2\omega^2$, where $\rho = n(r)/n_0\gamma(r)$. Hence, the $\eta_R(r)$ profile can be modified by (i) the relativistic transverse quiver motion of the electrons in the laser field, $\gamma = \gamma_\perp(r)$, where $\gamma_\perp = [1 + |\hat{a}_f(r)|^2/2]^{1/2}$, (ii) a preformed plasma density channel, $n = n^{(0)}(r)$, and (iii) the effects of a plasma wave, $n = n_0 + \delta n(r)$, where $\delta n = \delta n_0(r)\exp ik_p\zeta$ is the density oscillation. These three effects are responsible for relativistic optical guiding, density channel guiding, and the self–modulation of long laser pulses.

A. Relativistic Optical Guiding

In the standard theory of relativistic optical guiding [5,13,14], only the effects of the transverse quiver motion of the electrons are included in the expression for η_R, i.e., $n = n_0$ and $\gamma = \gamma_\perp(r)$. Analysis of the wave equation with an index of refraction of this form indicates that when the laser pulse power exceeds a critical power, $P \geq P_{crit}$, where $P_{crit} \simeq 17(\omega/\omega_p)^2$ GW, relativistic effects can prevent the diffraction of the laser pulse. The self–consistent, nonlinear theory developed in Refs. [6,9] showed, however, that relativistic optical guiding is ineffective in preventing the diffraction of sufficiently short pulses, $L \lesssim \lambda_p/(1+|\hat{a}_f|^2/2)^{1/2}$. This is due to the fact that the index of refraction becomes modified by the laser pulse on the plasma frequency time scale, not the laser frequency time scale. Typically, relativistic guiding only effects the body of long pulses, $L > \lambda_p$.

B. Long Pulse Self–Modulation

Recently, it was shown that long pulses, $L > \lambda_p$, with $P > P_{crit}$ can be subject to severe self–modulation [8,9,11]. Specifically, a plasma wave, excited by either the finite rise of the laser pulse envelope or by a forward Raman scattering (FRS) instability, can strongly affect the focusing properties of the pulse body. Consider a long laser pulse, $L \gg \lambda_p$, with $P = P_{crit}$ on which a finite wakefield (a plasma wave with phase velocity approximately

equal to the group velocity of the laser pulse) exists. The wakefield, which consists of a plasma density modulation of the form $\delta n = \delta n_0(r)\cos(k_p\zeta)$, modifies the plasma's refractive index [17]. In regions of a local density channel, i.e., where $\partial\delta n/\partial r > 0$, the radiation focuses. In regions where $\partial\delta n/\partial r < 0$, diffraction is enhanced. This causes the laser pulse envelope to become modulated at the plasma wavelength, which subsequently enhances the growth of the plasma wave, and the process proceeds in a highly nonlinear manner. In the limit $r_0 \gg \lambda_p$ and $P < P_{crit}$, in which the e–folding length of the standard FRS instability, L_{FRS}, is much less than the Rayleigh length, i.e., $L_{FRS} \ll Z_R$, the self–modulation process is adequately described by standard FRS theory. In the limit $P \geq P_{crit}$ and $L_{FRS} \gtrsim Z_R$, however, the modulation process is highly nonlinear with a growth rate much greater than that expected from standard FRS theory [11]. This results in a fully self–modulated laser pulse, composed of a series of laser "beamlets" of length $\simeq \lambda_p/2$, which can remain optically guided over several Rayleigh lengths. Associated with the periodic beamlet structure are large amplitude wakefields which can trap and accelerate a trailing electron beam. This process forms the basis of the self–modulated LWFA discussed below [11].

C. Tailored Pulse Propagation

A laser pulse with an appropriately tailored envelope can propagate many Rayleigh lengths without significantly altering its original profile [8-10]. Consider a long laser pulse, $L \gg \lambda_p$, in which the spot size is tapered from a large value at the front to a small value at the back, so that the laser power, $P \sim r_L^2|\hat{a}_f|^2$, is constant throughout the pulse and equal to P_{crit}. The leading portion ($\ll \lambda_p$) of the pulse will diffract as if in vacuum [6,8]. However, since r_L is large at the front of the pulse, the Rayleigh length is also large. Hence, the locally large spot size allows the pulse front to propagate a long distance, whereas the body of the pulse will be relativistically guided. Also, since $|\hat{a}_f|^2$ increases slowly throughout the pulse, detrimental wakefield effects (i.e., self–modulation) are reduced [8-10,21].

D. Plasma Density Channel Guiding

A preformed plasma density channel can guide short, intense laser pulses [7-9,17]. In the weak laser pulse limit, $|\hat{a}_f|^2 \ll 1$, the index of refraction is given by $\eta_R = 1 -$

$\omega_p^2\rho^{(0)}/2\omega^2$. Optical guiding requires $\partial\eta_R/\partial r < 0$, hence, a preformed density channel, $n^{(0)}(r) = n_0\rho^{(0)}(r)$, can prevent pulse diffraction. Analysis of the wave equation in the weak pulse limit indicates that a parabolic density channel will guide a Gaussian laser beam provided that the depth of the density channel [7-9,17] is $\Delta n = 1/\pi r_e r_L^2$, where $\Delta n = n^{(0)}(r_L) - n^{(0)}(0)$ and $r_e = e^2/m_e c^2$ is the classical electron radius. One possible method for creating a preformed density channel is to use the ponderomotive force of one or more additional laser beams.

IV. LWFA SIMULATIONS

To study laser pulse propagation and wakefield generation in plasma, the set of Maxwell–fluid equations, Eq. (5)-(7), are solved numerically. Specifically, the equation $\partial^2\psi/\partial\zeta^2 = G(\psi, |\hat{a}_f|^2)$ is solved for a given laser envelope, and the wave equation, Eq. (7), is solved to update the laser envelope, neglecting the $\partial^2/\partial\tau^2$ term. Retention of the $\partial^2/\partial\zeta\partial\tau$ term Eq. (7) is necessary to correctly describe the group velocity, $v_g < c$, of the laser pulse, the phase velocity of the wakefield, and the phase detuning of the accelerated electron beam [11,12]. To study the acceleration and trapping of electrons by the high–gradient wakefield, a particle code is used to evolve a distribution of non–interacting test electron beam particles in the time–resolved electric and magnetic wakefields of the simulation. Examples of three LWFA acceleration schemes will be presented, a channel–guided LWFA [9], a tailored–pulse LWFA [10], and a self–modulated LWFA [11]. In the channel–guided LWFA and the tailored-pulse LWFA simulations, in which phase detuning is not an issue, the term proportional to $\partial^2/\partial\zeta\partial\tau$ has also been neglected on the left side of the wave equation, Eq. (7).

A. Channel–Guided LWFA

The results of a channel–guided LWFA simulation [9] are shown in Figs. 1-3. In this example, the initial axial laser profile is given by $|\hat{a}_f(\zeta)| = a_0 \sin(-\pi\zeta/L)$ for $0 < -\zeta < L$, with $a_0 = 0.72$ and $L = 120$ μm (400 fs). Also, $\lambda = 1$ μm and $r_L = 60$ μm (Gaussian radial profile), which implies $Z_R = 1.1$ cm and $P = 40$ TW. The density on axis is chosen such that $L = \lambda_p$ ($n_0 = 7.8\times10^{16}$ cm^{-3}) and a preformed density channel with a parabolic profile is assumed with $\Delta n = 1/\pi r_e r_L^2 = 3.2\times10^{16}$ cm^{-3}.

Figure 1(a) shows the evolution of the laser spot size versus propagation distance, $c\tau$. The laser pulse remains well-guided by the density channel, the laser spot size exhibiting small oscillations about its initial value over the full $20Z_R = 23$ cm simulation length. After $c\tau = 20Z_R$, the pulse profile shows very little distortion from its initial profile. A surface plot of the electron density profile at $c\tau = 20Z_R$ is shown in Fig. 2. The initial, unperturbed parabolic profile can be seen at the right ($\zeta = 0$), and the distortion of the channel by the laser pulse, including the excitation of a large amplitude wakefield along the axis, is evident in the region $\zeta < 0$. In this example, nearly all the electrons have been expelled from the vicinity of the laser pulse. A plot of the axial electric field along the axis at $c\tau = 20Z_R$ is shown in Fig. 3. The effects of the wakefields on a continuous electron beam with an initial normalized emittance $\epsilon_n = 1.0$ mm-mrad, RMS radius $r_b = 10$ μm and energy $E_b = 2$ MeV was also simulated. After $c\tau = 20$ cm, approximately 70% of the beam electrons were trapped and accelerated. The peak electron energy increases nearly linearly with propagation distance with an average acceleration gradient of 5.25 GeV/m (1 GeV in 20 cm).

B. Tailored–Pulse LWFA

Simulation results for a LWFA utilizing a tailored laser pulse [10] are shown in Figs. 1,4 and 5. The initial normalized intensity profile, $|\hat{a}_f|^2$, is shown in Fig. 4(a). The local spot size at the front ($\zeta = 0$) of the pulse is large, $r_L \simeq 8\lambda_p$, and tapers down over $\zeta = -2\lambda_p$ to $r_L = \lambda_p$ (a Gaussian radial profile assumed throughout). The initial axial laser envelope is given by $|\hat{a}_f(\zeta)| = a_L \sin(-\pi\zeta/4\lambda_p)$ for $0 < -\zeta < 2\lambda_p$ such that $P = P_{crit}$ at each ζ slice, i.e., $r_L(\zeta)a_0(\zeta) = 0.9\lambda_p$. Also, $\lambda = 1$ μm and $\lambda_p = 30$ μm ($n_0 = 1.2 \times 10^{18}$ cm^{-3}, initially a uniform plasma), such that $P = P_{crit} = 16$ TW. This gives a peak value of $a_0 = 0.9$ at the back of the pulse where $r_L = \lambda_p$, which corresponds to a Rayleigh length of $Z_R = 0.28$ cm. The pulse intensity then terminates over a distance of $L_{fall} = \lambda_p/2$. The pulse energy is approximately 3 J and the pulse length is approximately $L = 2\lambda_p = 60$ μm (200 fs). Because $L_{fall} < \lambda_p$, a large amplitude wakefield will be excited behind the pulse.

Figure 4(b) shows the normalized intensity profile after propagating $c\tau = 10Z_R = 2.8$ cm. The pulse is somewhat distorted, but largely intact. The evolution of the pulse spot

size at the position of peak intensity verses propagation distance is shown in Fig. 1(b), indicating that guiding has been achieved over the $10Z_R$ simulation region. The axial electric field of the wake on axis after $c\tau = 10Z_R$ is shown in Fig. 5. The evolution of a continuous electron beam with an initial normalized emittance $\epsilon_n = 1.0$ mm-mrad, RMS radius $r_b = 5$ μm and energy $E_b = 2$ MeV was simulated using the self-consistent wakefields. After $c\tau = 2.8$ cm, approximately 60% of the beam electrons were trapped and accelerated. The peak energy of the beam electrons experienced an average gradient of 27 GeV/m (750 MeV in 2.8 cm).

C. Self-Modulated LWFA

The mechanism of long-pulse self-modulation can form the basis for a LWFA [11]. To operate in the self-modulated regime, it is necessary that (i) the pulse length be long compared to the plasma wavelength, $L > \lambda_p$, and (ii) the power be equal or greater than the critical power, $P \geq P_{crit}$. For fixed laser pulse parameters, i.e., fixed L and P, the self-modulated regime can be reach by operating at sufficiently high density, since $\lambda_p \sim 1/\sqrt{n_0}$ and $P_{crit} \sim 1/n_0$. The advantages of the self-modulated LWFA over the standard LWFA (in which $L \simeq \lambda_p$) are simplicity and enhanced acceleration. Simplicity in that a matching condition of $L \simeq \lambda_p$, a preformed density channel and/or special pulse tailoring are not required. Enhanced acceleration is achieved for several reasons: (i) The self-modulated LWFA operates at higher density, hence a larger wakefield will be generated, since $E_z \sim 1/\sqrt{n_0}$, as indicated by Eq. (2); (ii) since $P > P_{crit}$, the laser pulse will tend to focus to a higher intensity, thus increasing a_0 and E_z; (iii) the wakefield is resonantly excited, i.e., excited by a series of beamlets as opposed to a single pulse as in the standard LWFA; and (iv) relativistic optical guiding allows the modulated pulse structure to propagate for several Rayleigh lengths, thus extending the acceleration distance. The disadvantages of the self-modulated LWFA are (i) at higher densities the laser pulse group velocity ($\simeq$ the plasma wakefield phase velocity [12]) decreases and, hence, electron dephasing from the plasma wakefield can limit the acceleration distance, and (ii) the modulated pulse structure eventually diffracts.

The properties of the self-modulated LWFA are illustrated by the following simula-

tions. For fixed laser pulse parameters, two cases will be considered: (I) a standard LWFA in which $L \simeq \lambda_p$ and $P < P_{crit}$ and (II) a self–modulated LWFA, in which $L > \lambda_p$ and $P > P_{crit}$. The laser parameters for both these cases are identical: a Gaussian axial intensity profile with a pulse length $L = 90$ μm (300 fs), $\lambda = 1$ μm, $a_0 = 0.7$, $r_0 = 31$ μm (in vacuum), which corresponds to $Z_R = 3$ mm, $P = 10$ TW and a pulse energy of $W = 1.5$ J, well within the bounds of present technology. The simulation begins at $\tau = 0$ as the laser pulse enters the plasma, initially converging such that in vacuum it would focus to a minimum spot size of $r_0 = 31$ μm at $c\tau = 3Z_R$. The plasma density is initially increasing, reaching full density at $c\tau = 2Z_R$. The simulation continues until $c\tau = 10Z_R = 3$ cm. In both cases, the acceleration and trapping of a continuous electron beam with initial energy of 3 MeV and normalized emittance $\epsilon_n = 130$ mm-mrad is considered. The electron beam is initially converging such that in vacuum it would focus to a minimum RMS radius $r_b = 200$ μm at $c\tau = 3Z_R$. With such a large initial emittance, only a small fraction ($\sim 1\%$) of the particles will be trapped and accelerated.

For the standard LWFA, Case I, the requirement $L = \lambda_p = 90$ μm implies a density of $n_0 = 1.4 \times 10^{17}$ cm^{-3}. At this density, $P \ll P_{crit} = 140$ TW, such that relativistic guiding effects are unimportant. In fact, the presence of the plasma has little effect on the evolution of the laser pulse, which reaches a peak intensity of $|\hat{a}_f|^2 = 0.56$ at $c\tau = 3Z_R$. The evolution of the spot size, Fig. 1(c), is very close to vacuum diffraction. This is also evident in Fig. 6(a) (dashed line), where the peak accelerating field, plotted versus time, is symmetric about the focus, $c\tau = 3Z_R$. After $c\tau = 10Z_R = 3$ cm, a small fraction ($\sim 0.1\%$) of the test electron beam particles have been trapped and accelerated. At $c\tau = 2$ cm, the peak particle energy is 48 MeV, which implies an average acceleration of 2.4 GeV/m, as shown in Fig. 7(a) (dashed line).

For the self–modulated LWFA, Case II, the density is increased such that $P = 1.5P_{crit}$ $= 10$ TW, which implies $n_0 = 2.8 \times 10^{18}$ cm^{-3}, which is 20 times higher than in Case I. At this density $L > \lambda_p = 20$ μm, i.e., the laser pulse now extends over $\simeq 4.5\lambda_p$. Figure 8 shows the laser intensity at (a) $c\tau = 2Z_R$ and (b) $c\tau = 3.2Z_R$. The axial electric field on axis at $c\tau = 3.2Z_R$ is shown in Fig. 9. The laser pulse has become modulated (three peaks are observable, separated by λ_p) and the plasma wave is highly nonlinear.

In addition, relativistic optical guiding effects have focused the laser to a much higher intensity than was observed in Case I. The evolution of the laser spot size is shown in Fig. 1(d), indicating that the pulse has focused to a smaller spot size and remains guided over $\simeq 5.5Z_R$. A plot of the peak accelerating field versus time, Fig. 6(b) (solid line), shows that the highly nonlinear fields persist as the laser pulse is optically guided. A maximum accelerating field of $\simeq$ 130 GV/m was obtained. Approximately 2% of the test electron beam particles were trapped and accelerated. The peak particle energy of 430 MeV is observed at $c\tau = 6Z_R = 1.8$ cm. At $c\tau = 10Z_R = 3$ cm, however, the peak particle energy has dropped to 290 MeV due to the reduced group velocity of the laser pulse, which causes the electrons to slip out of phase with the wakefield and become decelerated. Figure 7(b) (solid line) shows acceleration to 430 MeV over 1.8 cm which gives an average gradient of 24 GeV/m. This is an order of magnitude increase compared to the standard LWFA of Case I.

V. CONCLUSION

The laser wakefield accelerator [4-11] is capable of generating ultrahigh accelerating and focusing fields over extended distances (many Rayleigh lengths), which can trap and accelerate a trailing electron beam. The large amplitude wakefields are generated by the ponderomotive forces associated with the envelope of the laser pulse. These forces can expel electrons from the vicinity of the laser pulse, thus exciting a large amplitude plasma wave (wakefield) with phase velocity near the speed of light. For a single laser pulse, the maximum wakefield amplitude results when the pulse length is approximately equal to the plasma wavelength, $L \simeq \lambda_p$. Diffraction places the most severe limitation on the pulse propagation distance, hence optical guiding is necessary to accelerate electrons to high energies [5]. Laser pulse diffraction can be prevented by the effects of relativistic optical guiding, preformed density channels, and/or appropriately tailored pulse profiles [5-11,13-17]. To study pulse propagation and wakefield generation, an axisymmetric Maxwell–fluid model was developed [8-11]. This model is valid for arbitrary laser intensities and can simulate laser propagation in plasma over large distances (many Rayleigh lengths).

Three possible LWFA configurations were simulated: (i) a channel–guided LWFA [9],

(ii) a tailored–pulse LWFA [10], and (iii) a self–modulated LWFA [11]. The channel–guided LWFA and tailored–pulse LWFA simulations demonstrate that a laser pulse can be optically guided over many Rayleigh lengths while generating large amplitude wakefields, which can trap and accelerate a test electron beam to high energies ($\sim$ 1 GeV). The self–modulated LWFA, a recently proposed configuration, is of particular interest, especially concerning the design of proof–of–principle LWFA experiments [11]. In the self–modulated LWFA, the plasma density is chosen to be sufficiently high so that the laser pulse is long compared to a plasma wavelength, $L > \lambda_p$, and the power exceed the critical power, $P > P_{crit}$. Previously it was believed that in the long–pulse regime, in which $|\partial \hat{a}_f/\partial\zeta| \sim L|\hat{a}_f|$ and $L \gg \lambda_p$, the plasma electrons respond adiabatically, and no significant wakefield would be generated. This, however, is not necessarily the case. When $L > \lambda_p$ and $P > P_{crit}$, the laser pulse can become strongly self–modulated at the plasma wavelength and large amplitude wakefields are resonantly excited. This results in enhanced wakefield amplitudes and enhanced acceleration in comparison to the standard LWFA (in which $L \simeq \lambda_p$). For the simulation presented in Section IV, electron acceleration was enhanced by an order of magnitude by operating in the self–modulated regime for fixed laser parameters, simply by increasing the ambient density by a factor of 20. The self–modulated LWFA has the additional advantage of simplicity, i.e., preformed density channels, pulse profile tailoring, and a matching condition of $L \simeq \lambda_p$ are not necessary. Hence, the self–modulated regime is well–suited for a proof–of–principle LWFA experiment.

ACKNOWLEDGMENTS

The authors wish to acknowledge useful conversations with D. Umstadter and G. Mourou of the University of Michigan. This work was supported by the Department of Energy and the Office of Naval Research.

REFERENCES

1. *Laser Acceleration of Particles*, Edited by P. Channell, AIP Conf. Proc. No. 91. (AIP, NY 1982); *Laser Acceleration of Particles*, Edited by C. Joshi and T. Katsouleas, AIP Conf. Proc. No. 130 (AIP, NY, 1985); *Advanced Accelerator Concepts*, Edited by F. Mills, AIP Conf. Proc. No. 156 (AIP, NY, 1986); *Advanced Accelerator Concepts*, Edited by C. Joshi, AIP Conf. Proc. No. 193 (AIP, NY, 1989); *Advanced Accelerator Concepts*, Edited by J. S. Wurtele, AIP Conf. Proc. (to be published).
2. D. Strickland and G. Mourou, Opt. Commun. **56**, 216 (1985); P. Maine, D. Strickland, P. Bado, M. Pessot and G. Mourou, IEEE J. Quantum Electron. **QE-24**, 398 (1988); M. Ferray, L. A. Lompre, O. Gobert, A. L'Huillier, G. Mainfray, C. Manus and A. Sanchez, Opt. Commun. **75**, 278 (1990); M. D. Perry. F. G. Patterson and J. Weston, Opt. Lett. **15**, 1400 (1990).
3. G. Mourou and D. Umstadter, Phys. Fluids B **4**, 2315 (1992); J. P. Watteau, G. Bonnaud, J. Coutant, R. Dautray, A. Decoster, M. Louis–Jacquet, J. Ouvry, J. Sauteret, S. Seznec, D. Teychenne, Phys. Fluids B **4**, 2217 (1992).
4. T. Tajima and J. M. Dawson, Phys. Rev. Lett. **43**, 267 (1979); L. M. Gorbunov and V. I. Kirsanov, Sov. Phys. JETP **66**, 290 (1987); V. N. Tsytovich, U. DeAngelis and R. Bingham, Comments Plasma Phys. Controlled Fusion **12**, 249 (1989); V. I. Berezhiani and I. G. Murusidze, Phys. Lett. A **148**, 338 (1990); T. C. Katsouleas, W. B. Mori, J. M. Dawson and S. Wilks, in SPIE Conf. Proc. **1229**, ed. by E. M. Campell (SPIE, Bellingham, WA, 1990), p. 98.
5. P. Sprangle, E. Esarey, A. Ting and G. Joyce, Appl. Phys. Lett. **53**, 2146 (1988); E. Esarey, A. Ting, P. Sprangle and G. Joyce, Comments Plasma Phys. Controlled Fusion **12**, 191 (1989).
6. P. Sprangle, E. Esarey and A. Ting, Phys. Rev. Lett. **64**, 2011 (1990); Phys. Rev. A **41**, 4463 (1990); A. Ting, E. Esarey and P. Sprangle, Phys. Fluids B **2**, 1390 (1990).
7. P. Sprangle and E. Esarey, Phys. Fluids B **4**, 2241 (1992).
8. P. Sprangle, E. Esarey, J. Krall and G. Joyce, Phys. Rev. Lett. **69**, 2200 (1992).
9. P. Sprangle, E. Esarey, J. Krall, G. Joyce and A. Ting, in *Advanced Accelerator Concepts*, Edited by J. S. Wurtele, AIP Conf. Proc. (to be published).

10. J. Krall, G. Joyce, P. Sprangle and E. Esarey, *Advanced Accelerator Concepts*, Edited by J. S. Wurtele, AIP Conf. Proc. (to be published).

11. J. Krall, A. Ting, E. Esarey and P. Sprangle, submitted to Phys. Rev. Lett.

12. C. D. Decker and W. B. Mori, submitted for publication.

13. A. G. Litvak, Sov. Phys. JETP **30**, 344 (1970); C. Max, J. Arons and A. B. Langdon, Phys. Rev. Lett. **33**, 209 (1974); G. Schmidt and W. Horton, Comments Plasma Phys. Controlled Fusion **9**, 85 (1985); P. Sprangle, C. M. Tang and E. Esarey, IEEE Trans. Plasma Sci. **PS-15**, 145 (1987); E. Esarey, A. Ting and P. Sprangle, Appl. Phys. Lett. **53**, 1266 (1988); W. B. Mori, C. Joshi, J. M. Dawson, D. W. Forslund and I. M. Kindel, Phys. Rev. Lett. **60**, 1298 (1988); P. Gibbon and A. R. Bell, Phys. Rev. Lett. **61**, 1599 (1988); C. J. McKinstrie and D. A. Russell, Phys. Rev. Lett. **61**, 2929 (1988).

14. G. Z. Sun, E. Ott, Y. C. Lee and P. Guzdar, Phys. Fluids **30**, 526 (1987); T. Kurki-Suonio, P. J. Morrison and T. Tajima, Phys. Rev. A **40**, 3230 (1989); A. B. Borisov, A. V. Borovskiy, V. V. Korobkin, A. M. Prokhorov, C. K. Rhodes and O. B. Shiryaev, Phys. Rev. Lett. **65**, 1753 (1990); P. Sprangle, A. Zigler and E. Esarey, Appl. Phys. Lett. **58**, 346 (1991); A. B. Borisov, A. V. Borovskiy, O. B. Shiryaev, V. V. Korobkin, A. M. Prokhorov, J. C. Solem, T. S. Luk, K. Boyer, and C. K. Rhodes, Phys. Rev. A **45**, 5830 (1992).

15. T. M. Antonsen, Jr. and P. Mora, Phys. Rev. Lett. **69**, 2204 (1992).

16. X. L. Chen and R. N. Sudan, submitted to Phys. Fluids.

17. E. Esarey, A. Ting and P. Sprangle, in *Advanced Accelerator Concepts*, Edited by C. Joshi, AIP Conf. Proc. No. 193 (AIP, NY, 1989), p. 71; E. Esarey and A. Ting, Phys. Rev. Lett. **65**, 1961 (1990).

18. P. Sprangle and E. Esarey, Phys. Rev. Lett. **67**, 2021 (1991); E. Esarey and P. Sprangle, Phys. Rev. A **45**, 5872 (1992).

19. C. B. Darrow, C. Coverdale, M. D. Perry, W. B. Mori, C. Clayton, K. Marsh and C. Joshi, Phys. Rev. Lett. **69**, 442 (1992); W. P. Leemans, C. E. Clayton, W. B. Mori, K. A. Marsh, P. K. Kaw, A. Dyson, C. Joshi and J. M. Wallace, Phys. Rev. A **46**, 1091 (1992).

20. J. M. Rax and N. J. Fisch, Phys. Fluids B **4**, 1323 (1992).

21. A somewhat analogous concept for electron beam drivers has been examined by P. Chen, J. J. Su, J. M. Dawson, K. L. F. Bane and P. B. Wilson, Phys. Rev. Lett. **56**, 1252 (1986).

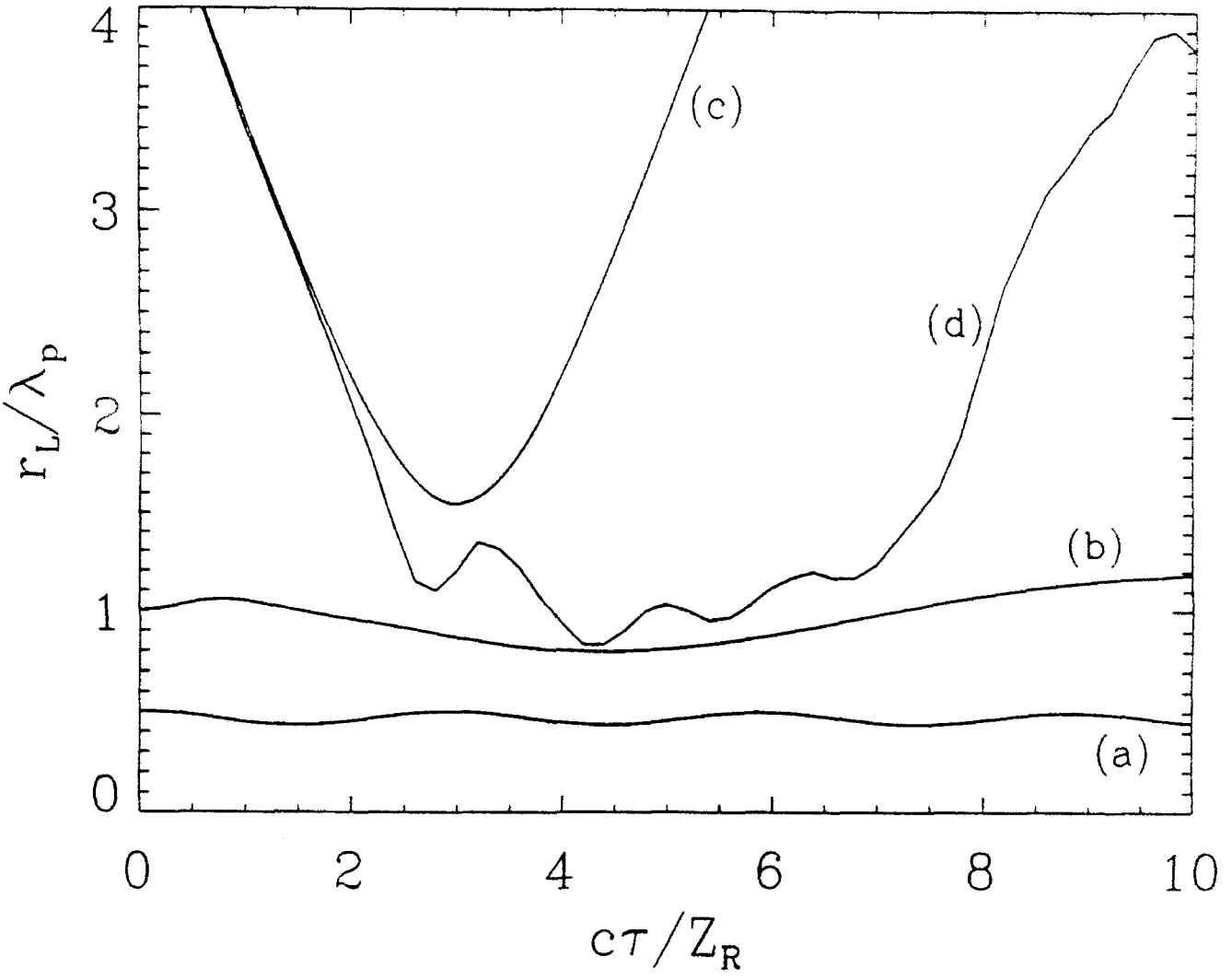

Fig. 1. Laser spot size normalized to the plasma wavelength, r_L/λ_p, at the position of peak intensity, versus propagation distance normalized to the Rayleigh length, $c\tau/Z_R$, for (a) the channel–guided LWFA, (b) the tailored–pulse LWFA, (c) vacuum diffraction for the parameters of the self–modulated LWFA, and (d) the self–modulated LWFA.

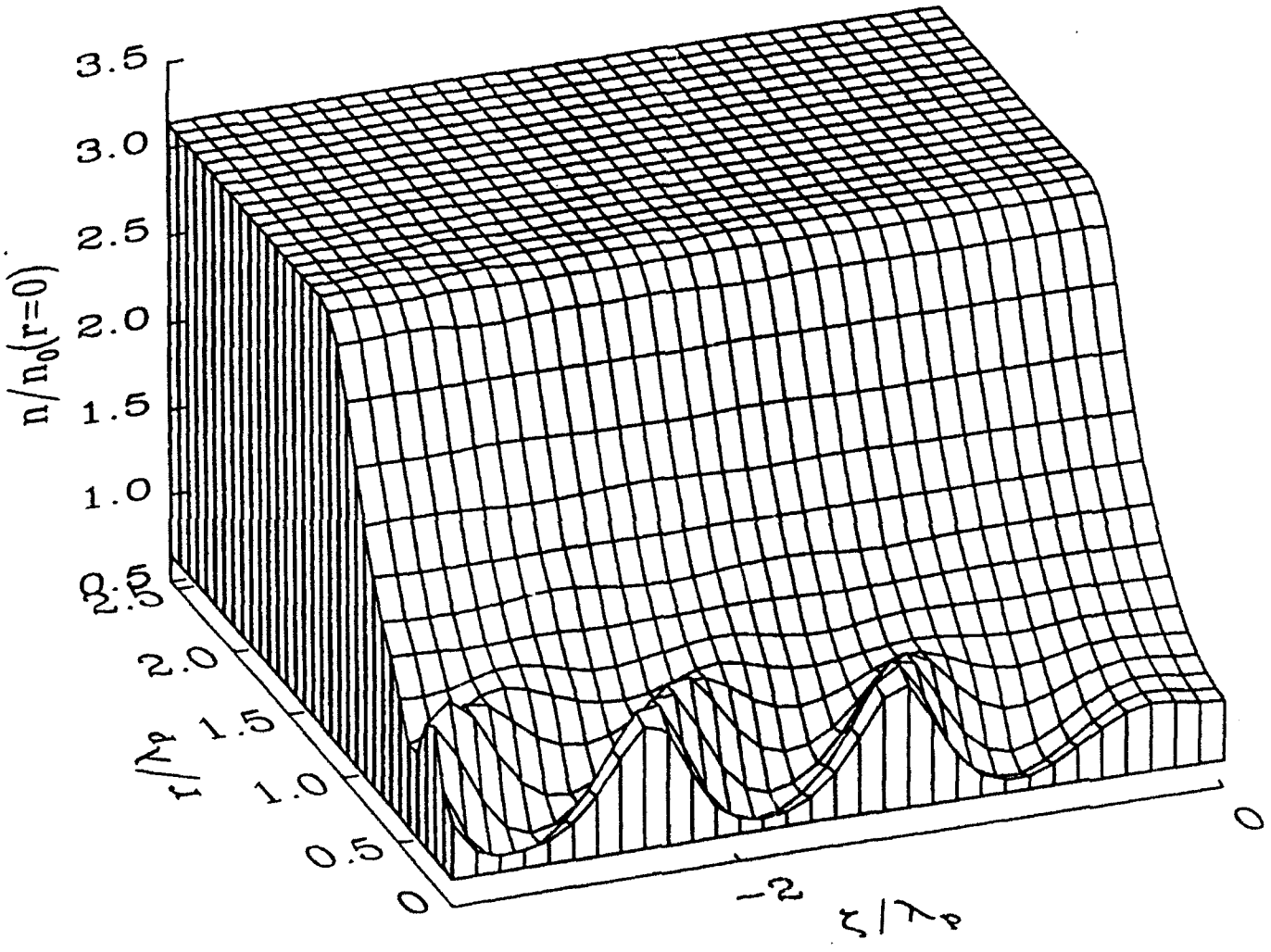

Fig. 2. Surface plot of the plasma electron density n/n_0 at $c\tau = 20Z_R$ for the channel-guided LWFA. The initial density profile is parabolic with a depth given by $\Delta n = 1/\pi r_e r_L^2$.

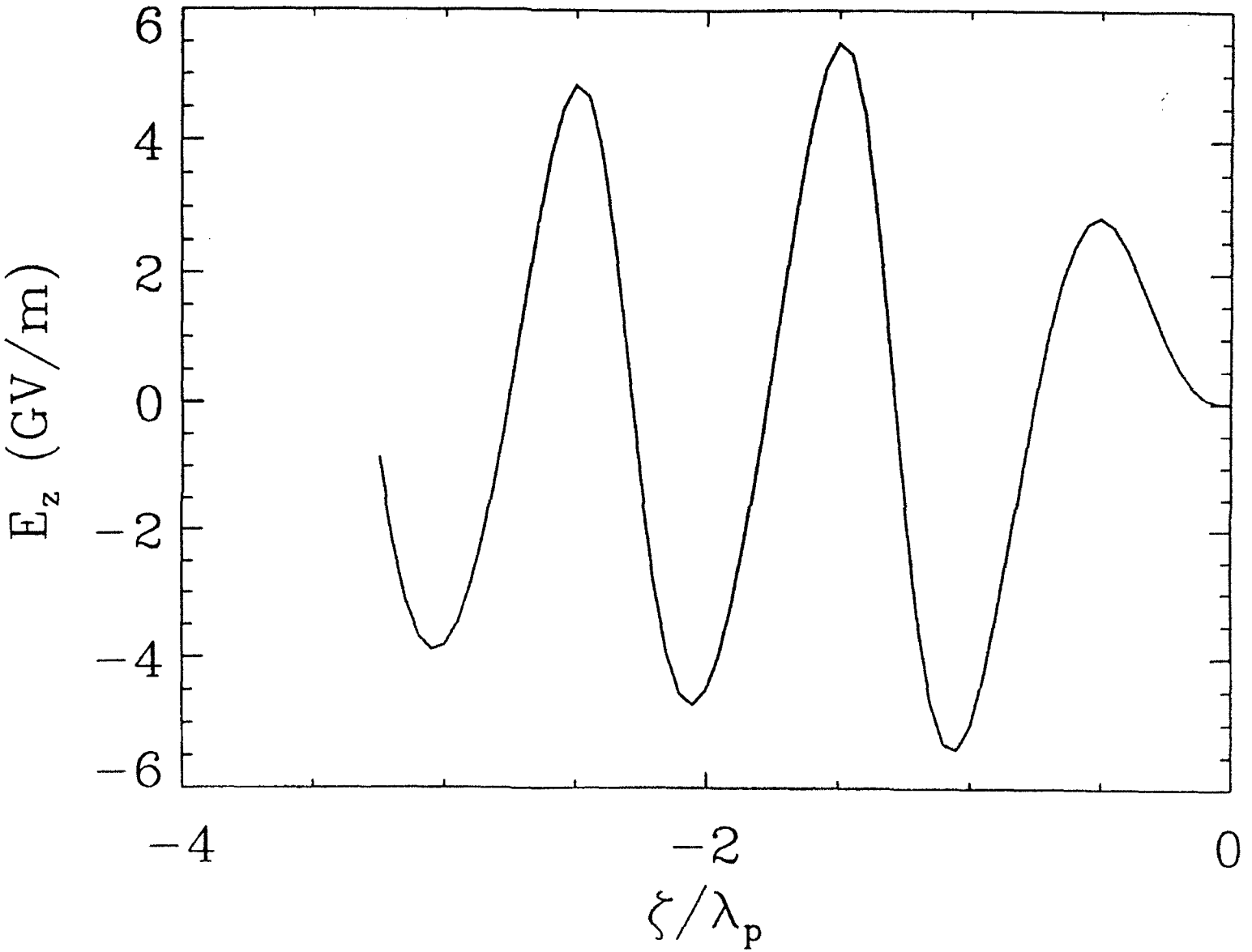

Fig. 3. Axial electric field E_z on axis at $c\tau = 20Z_R$ for the channel-guided LWFA.

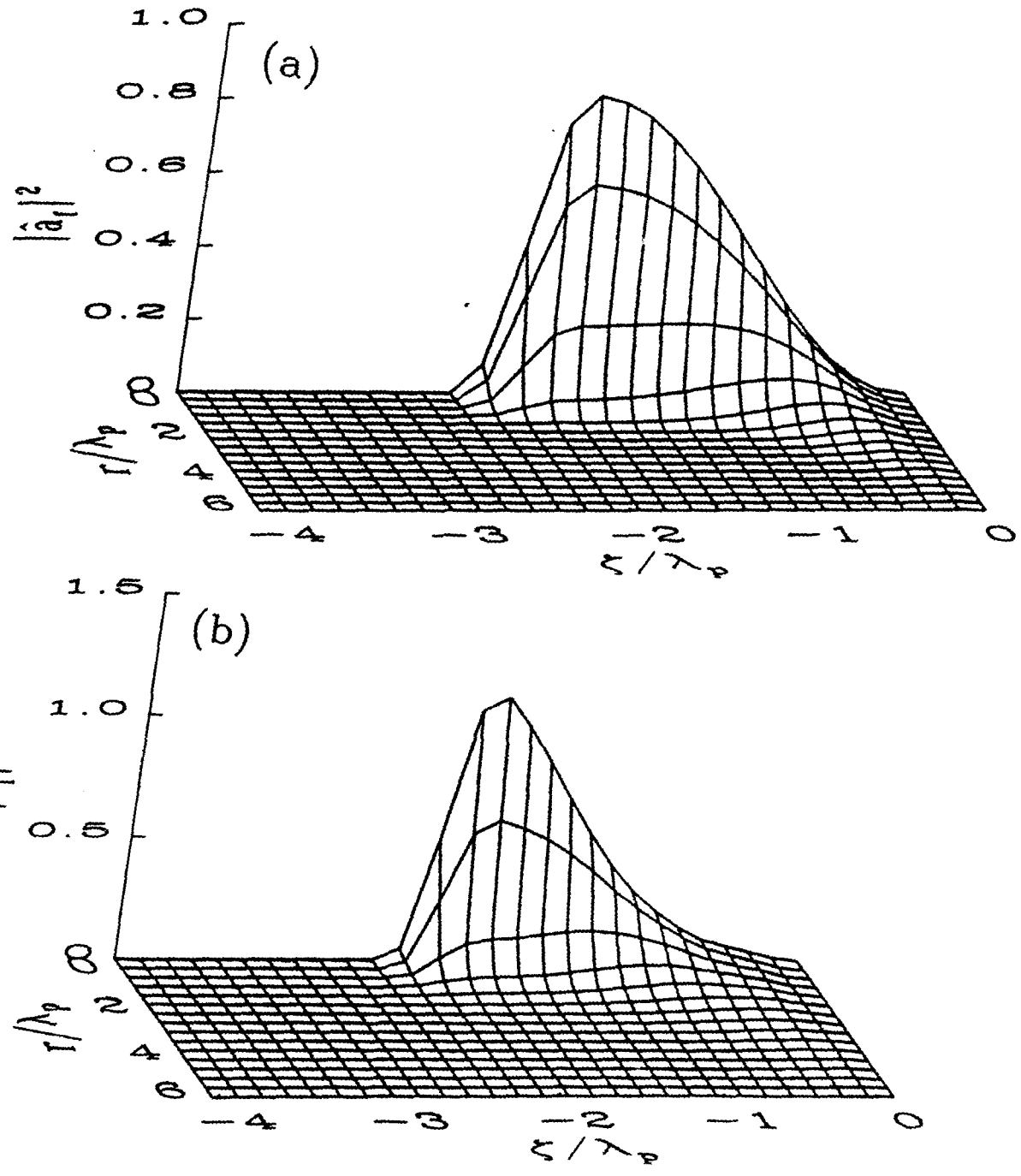

Fig. 4. Surface plot of the normalized laser intensity, $|\tilde{a}_f^*|$, at (a) $\tau = 0$ and at (b) $c\tau = 10Z_R$ for the tailored–pulse LWFA.

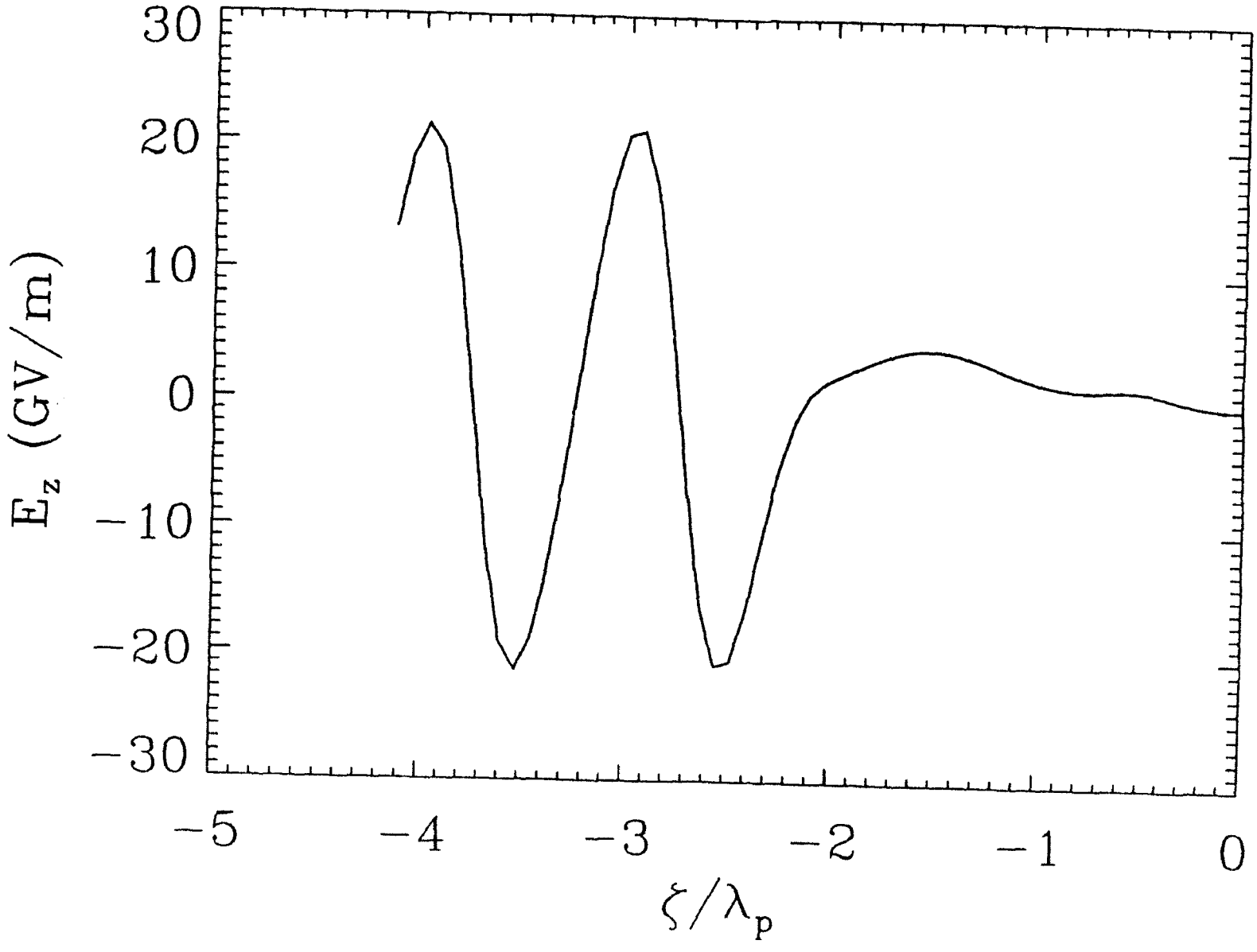

Fig. 5. Axial electric field E_z on axis at $c\tau = 10Z_R$ for the tailored–pulse LWFA.

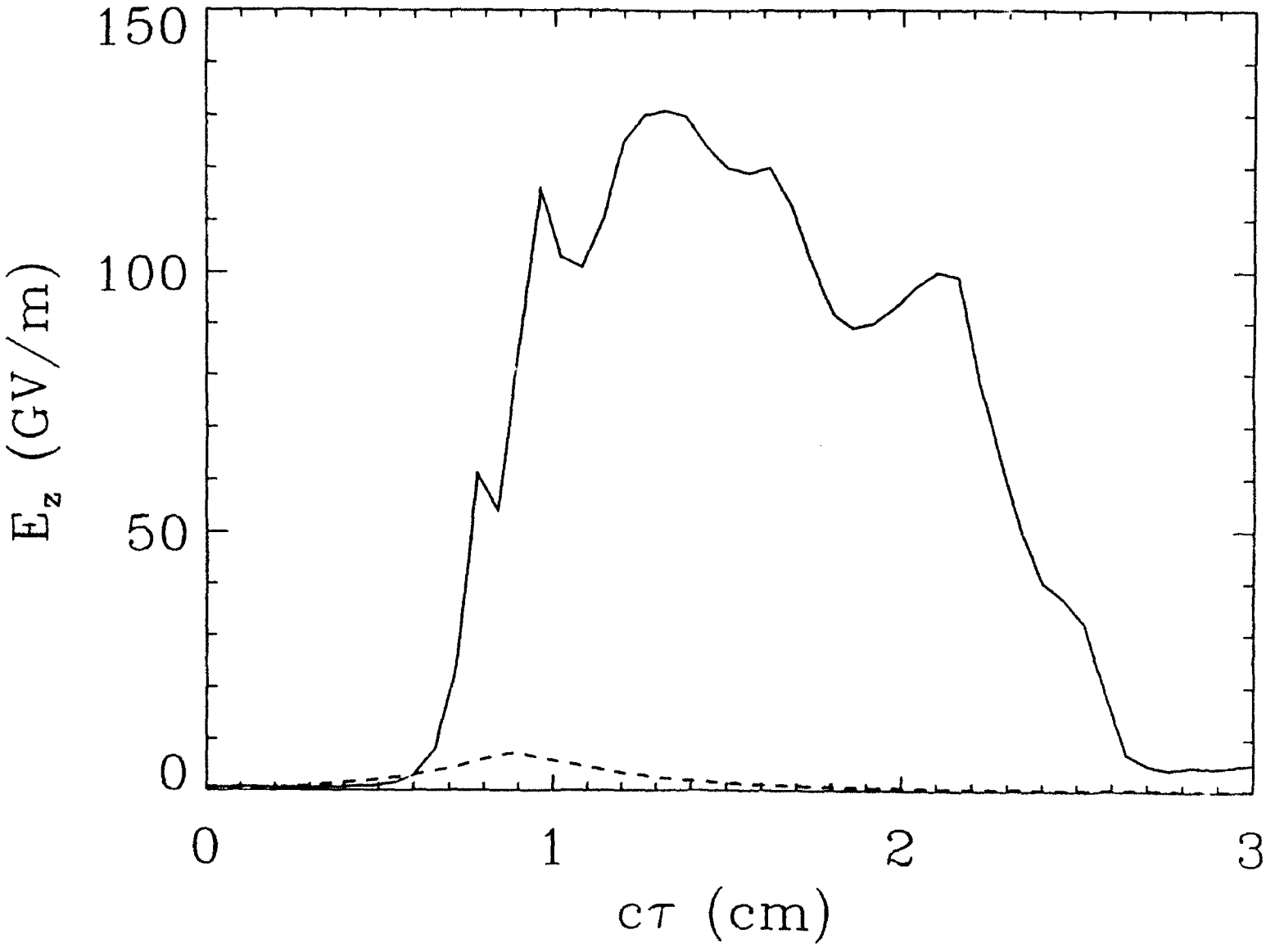

Fig. 6. Peak axial electric field, E_z, verses propagation distance, $c\tau$, for (a) the standard LWFA (Case I), dashed line; and (b) the self-modulated LWFA (Case II), solid line.

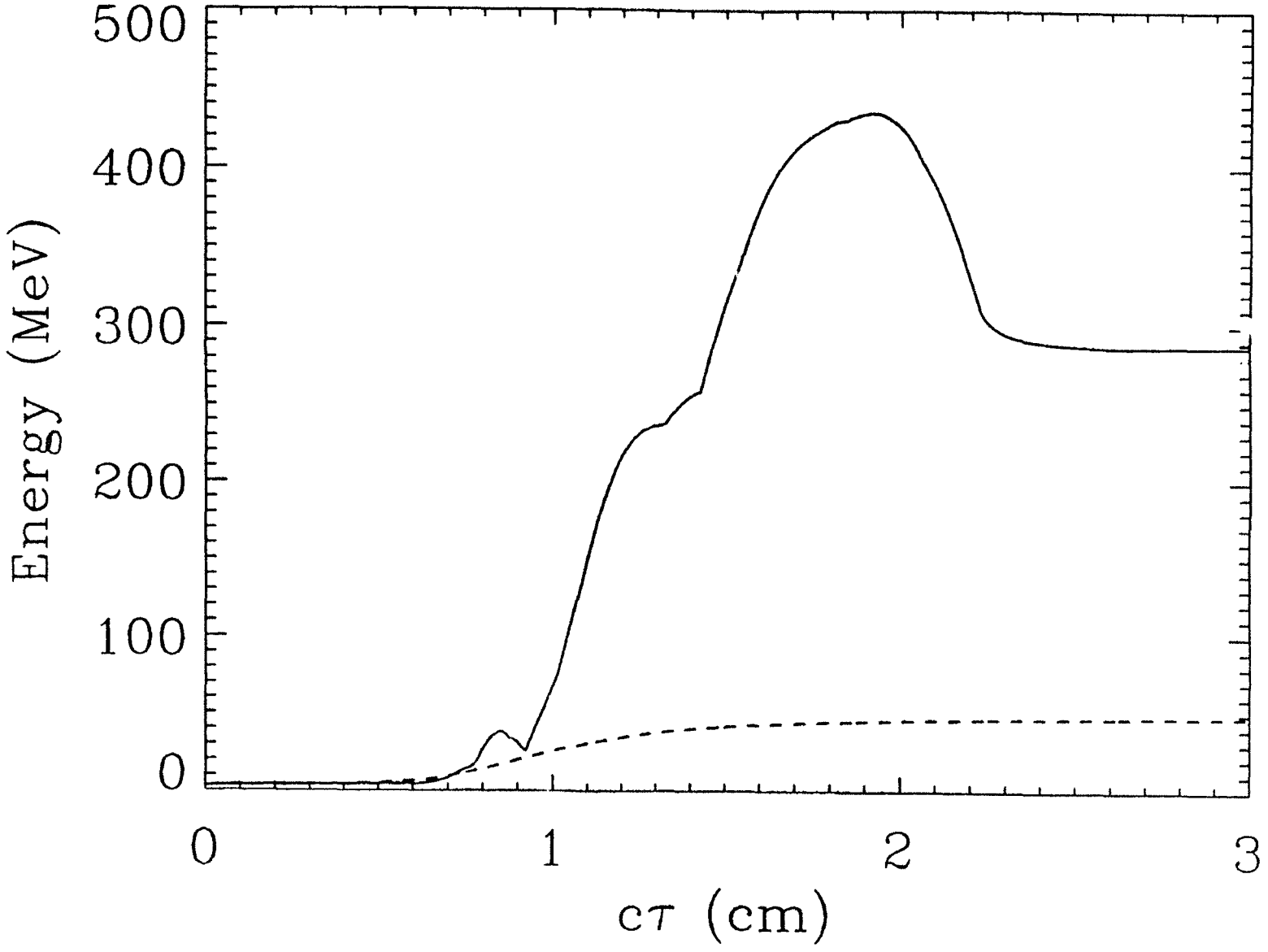

Fig. 7. Peak energy of the trapped electrons verses propagation distance, $c\tau$, for (a) the standard LWFA (Case I), dashed line; and (b) the self-modulated LWFA (Case II), solid line.

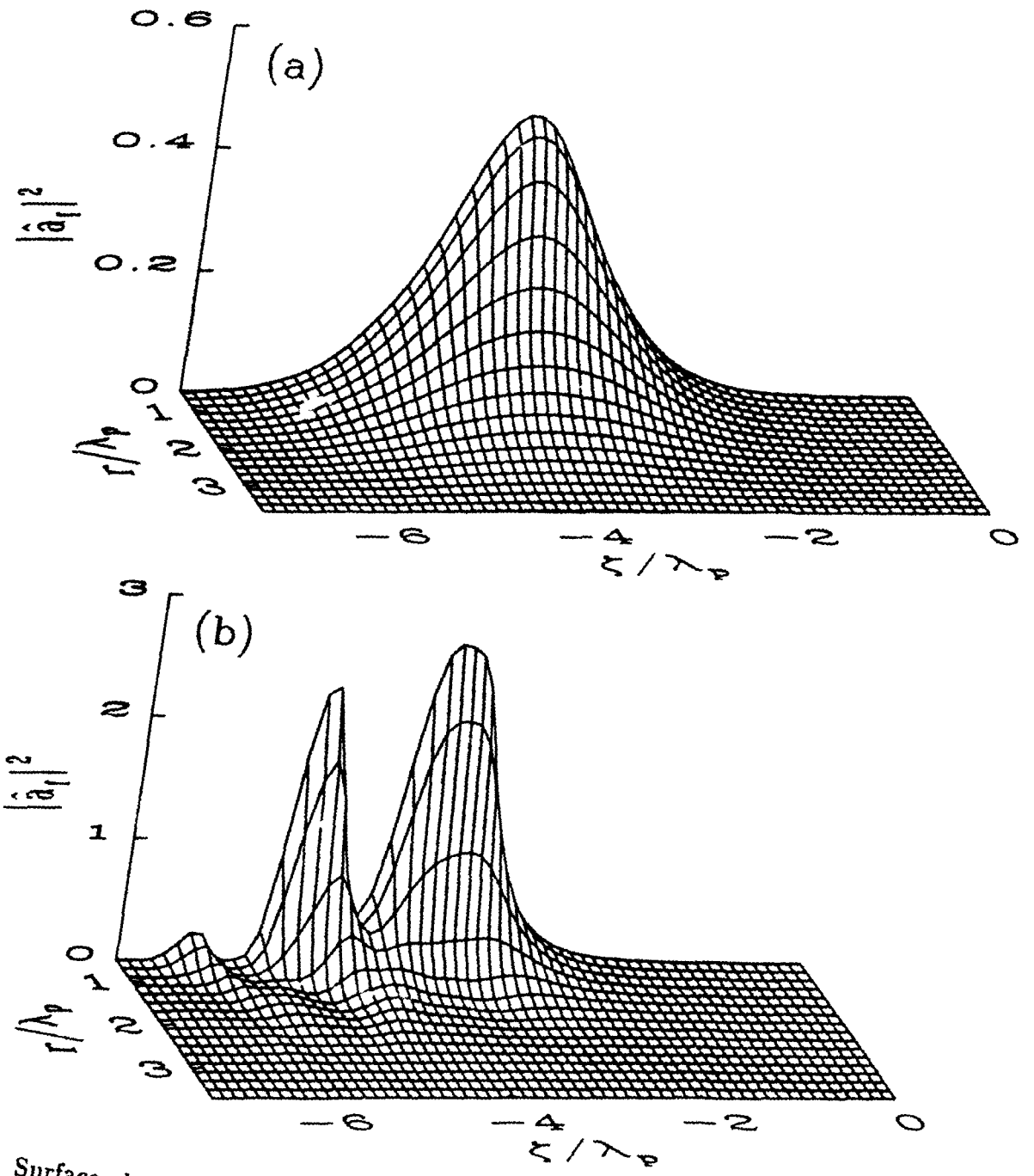

Fig. 8. Surface plot of the normalized laser intensity, $|\hat{a}_f^2|$, (a) entering the plasma ($c\tau = 2Z_R$) and (b) near the laser focus ($c\tau = 3.2Z_R$) for the self-modulated LWFA.

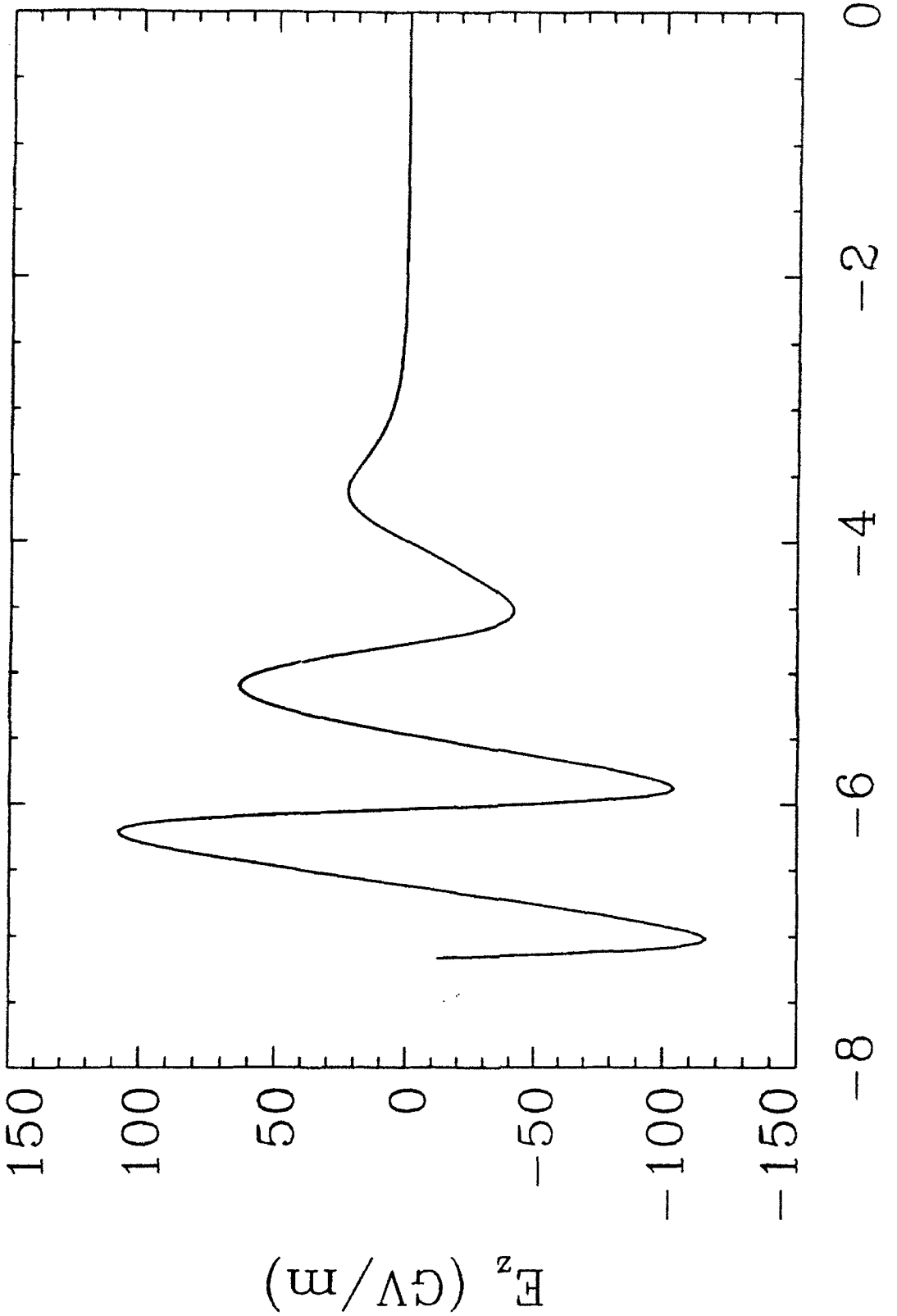

Fig. 9. Axial electric field E_z on axis at $cT = 3.2Z_R$ for the self-modulated LWFA.